

Structural and Functional Characterization of the Hazelnut Allergen Cor a 8

Lesa R. Offermann,^{†,‡} Merima Bublin,[§] Makenzie L. Perdue,[†] Sabine Pfeifer,[§] Paweł Dubielka,[§] Tomasz Borowski,[#] Maksymilian Chruszcz,^{*,†} and Karin Hoffmann-Sommergruber^{*,§}

[†]Department of Chemistry and Biochemistry, University of South Carolina, Columbia, South Carolina 29208, United States

[§]Department of Pathophysiology and Allergy Research, Center for Pathophysiology, Infectiology and Immunology, Medical University of Vienna, Vienna, Austria

[#]Jerzy Haber Institute of Catalysis and Surface Chemistry, Polish Academy of Sciences, Kraków, Poland

[‡]Department of Chemistry, Davidson College, Davidson, North Carolina 28035, United States

ABSTRACT: Nonspecific lipid transfer proteins (nsLTPs) are basic proteins, stabilized by four disulfide bonds, and are expressed throughout the plant kingdom. These proteins are also known as important allergens in fruits and tree nuts. In this study, the nsLTP from hazelnuts, Cor a 8, was purified and its crystal structure determined. The protein is stable at low pH and refolds after thermal denaturation. Molecular dynamics simulations were used to provide an insight into conformational changes of Cor a 8 upon ligand binding. When known epitope areas from Pru p 3 were compared to those of Cor a 8, differences were obvious, which may contribute to limited cross-reactivity between peach and hazelnut allergens. Differences in epitope regions may contribute to limited cross-reactivity between Cor a 8 and nsLTPs from other plant sources. The structure of Cor a 8 represents the first resolved structure of a hazelnut allergen.

KEYWORDS: *allergen, food allergy, hazelnut, nonspecific lipid transfer protein, protein crystallization*

INTRODUCTION

As the number of people affected by food allergies increases worldwide, with its prevalence estimated to be between 1 and 8% of the world's population,^{1,2} hazelnut (*Corylus avellana*) continues to lead as one of the most common allergen sources.^{3–6} Currently (June 2015), 10 allergens from *C. avellana* are registered with the Allergen Nomenclature Sub-Committee of the International Union of Immunological Societies (IUIS),⁷ belonging to a variety of protein families. However, five of these allergens (Cor a 1,⁸ Cor a 8,⁹ Cor a 9,¹⁰ Cor a 11,¹¹ and Cor a 14^{10,12}) are considered to be the major culprits associated with reactions in patients sensitized to hazelnut. In birch endemic areas, hazelnut allergy has mainly been associated with cross-reactive IgE to Bet v 1 and Bet v 2, usually causing mild symptoms known as oral allergy syndrome. The cross-reactive allergens in hazelnut are Cor a 1.04 (Bet v 1 homologue) and Cor a 2 (profilin).⁸ In areas lacking exposure to birch pollen (e.g., southern Europe), hazelnut allergies are mostly associated with more severe reactions¹³ and linked to sensitization to the nonspecific lipid transfer protein (nsLTP) Cor a 8.¹⁴

Nonspecific lipid transfer proteins are thought to be involved in plant defense against pathogens and environmental stress.^{15,16} They were first named for their ability to mediate the transfer of phospholipids between membranes *in vitro* and are small proteins with molecular masses of 9000 Da (nsLTP1) and 7000 Da (nsLTP2), basic isoelectric points, and a common α -helical structure.^{17,18} Cor a 8, along with other allergens identified as nsLTPs, has been classified as a member of the 9000 Da plant nsLTP1 subfamily, the members of which are expressed throughout the plant tissues but most notably found in edible parts.¹⁶ They are characterized by a typical cysteine

pattern forming disulfide bonds having strictly conserved connectivities, forming a stable, compact barrel-like structure, which is essential for lipid binding.¹⁹ This structural feature facilitates resistance to thermal treatment and digestion, which could explain their involvement in more severe allergic reactions.^{20,21}

Several three-dimensional structures of this family have been solved by NMR and X-ray crystallography, demonstrating that their overall structures are very similar. However, despite this common feature, nsLTPs display low sequence identities. It has been shown that nsLTPs from distantly related species do not cross-react to the same extent as members belonging to the same plant family, reflecting their phylogenetic relationship.^{22–24} Therefore, reliable structures of important nsLTP allergens are needed as a molecular basis for the identification of surface areas representing putative additional epitopes. Due to their association with more severe reactions and their presence among several different species of plant foods, nsLTPs seem to be promising targets for diagnostic tools and potential immunotherapy.^{9,16}

In this study we determined the structure of Cor a 8, an important food allergen from hazelnut, by X-ray crystallography and compared it with already known structures of the nsLTP family to get a deeper insight into the structural determinants that are responsible for cross-reactivity. Cor a 8 represents the

Received: July 20, 2015

Revised: September 23, 2015

Accepted: September 28, 2015

Published: September 28, 2015

first hazelnut allergen with a resolved three-dimensional structure.

MATERIALS AND METHODS

Protein Purification. Shelled, raw hazelnuts were frozen, ground in a blender, and defatted by extraction with hexane. Proteins from dried hazelnut flour were extracted with 10 volumes of extraction buffer (20 mM sodium acetate, pH 4.5, containing 0.5 M NaCl and 3% polyvinyl polypyrrrolidone). Globulins were removed by precipitation with cold methanol (60%, v/v), and prolamins were precipitated with acetone. After removal of the 2S albumin fraction by anion exchange chromatography (10 mL of Q sepharose; GE Healthcare, Little Chalfont, UK), Cor a 8 was purified from the flow-through by cation exchange chromatography. The flow-through was dialyzed against 20 mM sodium acetate, pH 7.6, and loaded onto a prepacked 1 mL Mono S column (GE Healthcare). Proteins bound to the column were eluted by a linear gradient of increasing concentrations (0–20%) of 1 M NaCl with a flow rate of 1 mL/min. Both columns were attached to a GE ÄKTA FPLC system (GE Healthcare). Fractions were analyzed by Coomassie-stained 15% SDS-PAGE.

Circular Dichroism (CD) Spectroscopy. CD spectra of native Cor a 8 (0.2 μ g/ μ L in 10 mM sodium phosphate buffer, pH 2.5 or 7.5) were measured from 190 to 260 nm on a Jasco J-810 spectropolarimeter (Jasco International Co., Tokyo, Japan) at 20 °C using a 1 mm path length quartz cell. The effect of heating (2 °C/min) was measured at 222 nm. Spectra represent the average of four accumulations collected at 100 nm/min with a 2 s time constant, 0.5 nm resolution, and sensitivity of ± 100 mdeg.

N-Terminal Sequencing by Edman Degradation. The N-terminal sequence was determined using an Applied Biosystems Procise 491 sequencer (Applied Biosystems, Foster City, CA, USA). Cor a 8 (100 pmol) was adsorbed onto a Proscorb cartridge and subjected to sequence analysis.

MALDI-TOF-MS. For mass determination nonreduced Cor a 8 was spotted with α -cyano-4-hydroxycinnamic acid onto a ground steel MALDI target plate and measured in linear mode on a MALDI-TOF mass spectrometer (Microflex, Bruker Daltonics, Bremen, Germany).

Crystallization, Data Collection, and Processing. Crystallization experiments were performed at room temperature using the hanging-drop vapor diffusion method and screw-top hanging drop plates (Molecular Dimensions, Altamonte Springs, FL, USA). Purified, natural Cor a 8 in 20 mM Tris, pH 7.5, was mixed with well solution (0.49 M sodium phosphate monobasic monohydrate, 0.91 M potassium phosphate dibasic, pH 6.9) in a 1:1 ratio. Crystals were cryo-protected with well solution and cooled in liquid N₂. Data were collected from single crystals at 100 K at SER-CAT 22BM beamline at the Advanced Photon Source (APS), Argonne National Laboratory (ANL). Crystals belonged to the P₂1 spacegroup, and the protein crystallized with two molecules per asymmetric unit (AU). Data were processed with the HKL-2000 software package.²⁵ Data collection statistics are reported in Table 1.

Structure Determination and Refinement. The structure of Cor a 8 was solved by molecular replacement using nsLTPs Pru p 3 from peach (PDB ID 2ALG) as the start model. Molecular replacement was performed with HKL-3000²⁶ integrated with MOLREP²⁷ and selected programs from the CCP4 package.²⁸ Models were rebuilt using COOT,²⁹ Buccaneer,³⁰ and ARP/wARP³¹ and refined with RE-FMAC.³² MOLPROBITY³³ and ADIT³⁴ were used for structure validation. Refinement statistics are summarized in Table 1.

Molecular Dynamics Simulations. Molecular force fields of lauric acid anion and *n*-heptane were described with the general amber force field (GAFF), whereas for the proteins, the amber force field ff03.r1 was employed. *n*-Heptane molecule and laureate anion were first optimized in extended conformations in vacuum at the B3LYP/6-31G(d,p) level, and then the electrostatic potential around them was computed at the level that is consistent with the GAFF, that is, HF/6-31G(d). Quantum chemical computations were performed with the Gaussian 09 suite of programs.³⁵ From the electrostatic potential RESP atomic charges were

Table 1. Crystallographic Data and Refinement Statistics for Cor a 8^a

PDB code	4XUW
Data collection	
wavelength (Å)	1.00
unit cell (<i>a</i> , <i>b</i> , <i>c</i> ; β) (Å; deg)	39.7, 30.8, 56.2; 108.9
space group	P2 ₁
solvent content (%)	28
protein chains in AU	2
resolution range (Å)	50.0–1.10
highest resolution shell (Å)	1.12–1.10
unique reflections	47711 (1266)
redundancy	7.0 (4.1)
completeness (%)	90.7 (49.1)
<i>R</i> _{merge} (%)	5.2 (15.7)
av <i>I</i> / σ (<i>I</i>)	37.4 (8.5)
Refinement	
<i>R</i> (%)	14.2
<i>R</i> _{free} (%)	17.7
mean <i>B</i> value (Å ²)	20.2
<i>B</i> from Wilson plot (Å ²)	14.4
RMS deviation bond lengths (Å)	0.02
RMS deviation bond angles (deg)	2.3
no. of amino acid residues	184
no. of water molecules	308
Ramachandran plot	
most favored regions (%)	98
additional allowed regions (%)	2

^aValues in parentheses refer to the highest resolution shell.

fitted with the use of antechamber and resp programs from the AmberTools package.³⁶

The ionization state of individual protein residues was tested with PROPKA 3.1 software.³⁷ For pH 7 all residues were predicted to be in their standard ionization state (N- and C-termini all LYS, ARG, and ASP charged).

Initial coordinates of the proteins were taken from PDB 2BSS for Pru p 3 and from PDB 4XUW for Cor a 8, respectively (chains A). The N-terminal Met residue of the Pru p 3 structure was removed, as it was added to the protein due to its heterologous expression in a bacterial host. Protein molecules were subsequently placed in a periodic box filled with explicit water molecules described with the TIP3P model³⁸ and the appropriate number of chloride anions to compensate the charge of the protein or protein/laureate complex. The box was chosen such that its edge was 10 Å away from the protein surface in either direction. The system was first minimized in three steps: 5000 steps with protein atoms restrained with 500 kcal/mol Å² harmonic constant, 5000 steps with 10 kcal/mol Å² harmonic restraint on protein, and then 10000 steps of an unrestrained minimization. The minimized system was heated from 0 to 300 K during a 50 ps NV dynamics, and then its density was equilibrated in a 0.5 ns NPT dynamics; in both steps protein backbone atoms were restrained with 1 kcal/mol Å². Subsequent unrestrained NPT (*T* = 300 K, *p* = 1 atm) dynamics simulation spanned 150 ns for each system, with a snapshot saved every 10 ps. Integration time step was 2 fs, SHAKE algorithm was used to constrain bonds of hydrogen atoms, and temperature and pressure were controlled with the Langevin dynamics and isotropic position scaling algorithm, respectively. MD simulations were conducted with the Amber12 suite with a GPU version of the PMEMD program.^{39,40} Snapshots of the last 10 ns of simulations were clustered with the average linkage algorithm applied to Ca carbons of the protein backbone. Representative structures of dominating clusters were used for structure comparisons.

Other Computational Calculations. Protein anisotropic refinement validation and analysis tool (PARVATI) was used to validate anisotropic displacement parameters.^{41,42} The SSM algorithm⁴³ in COOT was used to superpose protein models. All figures containing

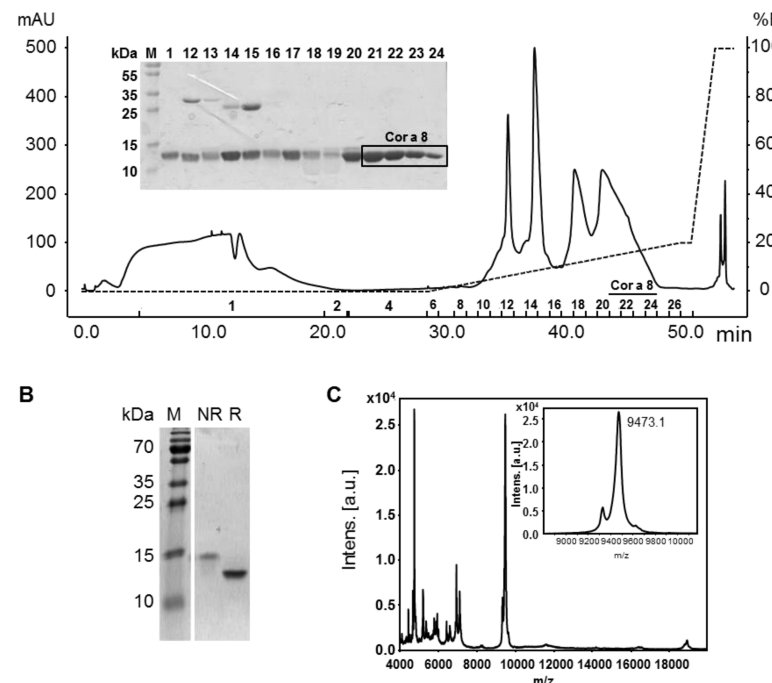


Figure 1. Purification of Cor a 8: (A) cation exchange chromatography of the hazelnut prolamin extract and Coomassie-stained 15% SDS-PAGE of Cor a 8-containing fractions; (B) 15% SDS-PAGE of purified Cor a 8 under nonreducing (NR) and reducing (R) conditions; (C) mass spectrum of Cor a 8.

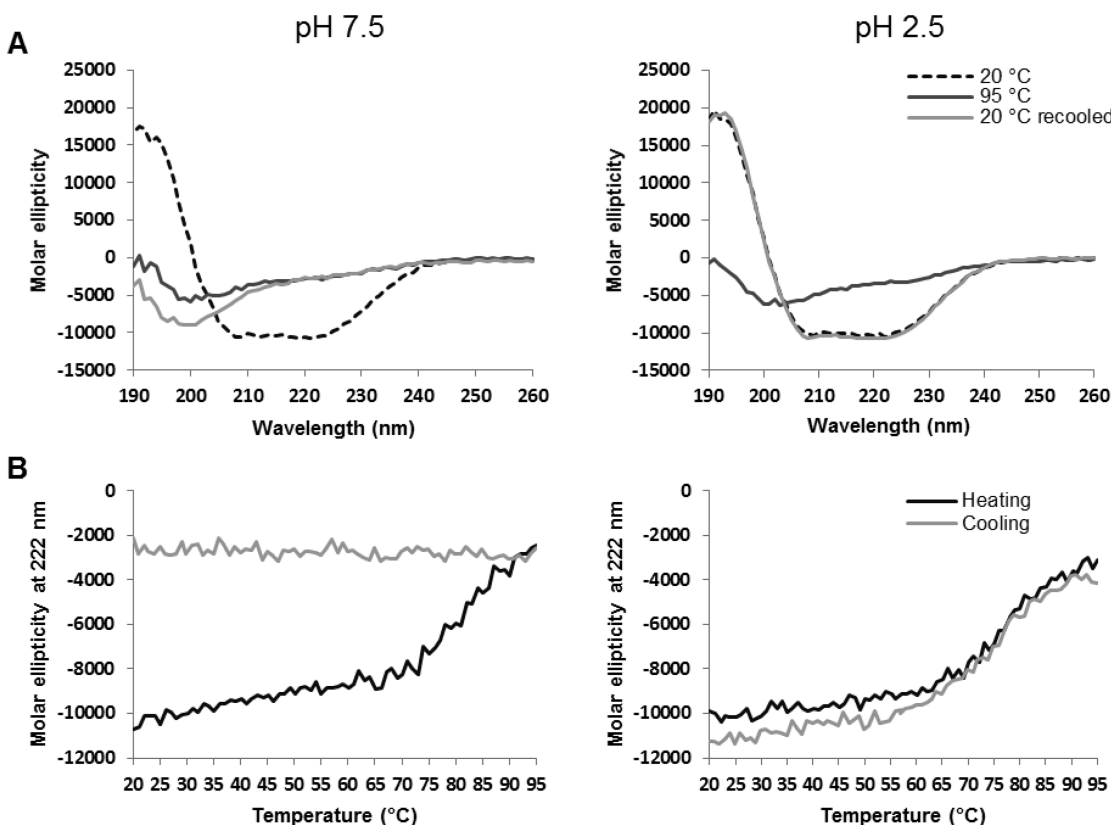


Figure 2. Far-UV CD spectra of Cor a 8: (A) spectra of Cor a 8 at room temperature (dotted line), after heating to 95 °C (dark gray line), and after recooling to room temperature (light gray line) at pH 2.5 and 7.5, respectively; (B) change in molar ellipticity at 222 nm during heating and cooling.

protein structures were prepared with PyMOL⁴⁴ or Chimera.⁴⁵ PDBePISA was used to calculate the probability of quaternary structure.⁴⁶ The Dali server⁴⁷ was used to identify structurally similar proteins. The ConSurf server was used to map sequence conservation on the structure of Cor a 8.⁴⁸

RESULTS

Purification and Characterization of Natural Cor a 8.

Cor a 8 was separated from the prolamin fraction of hazelnut extract by using ion exchange chromatography techniques. SDS-

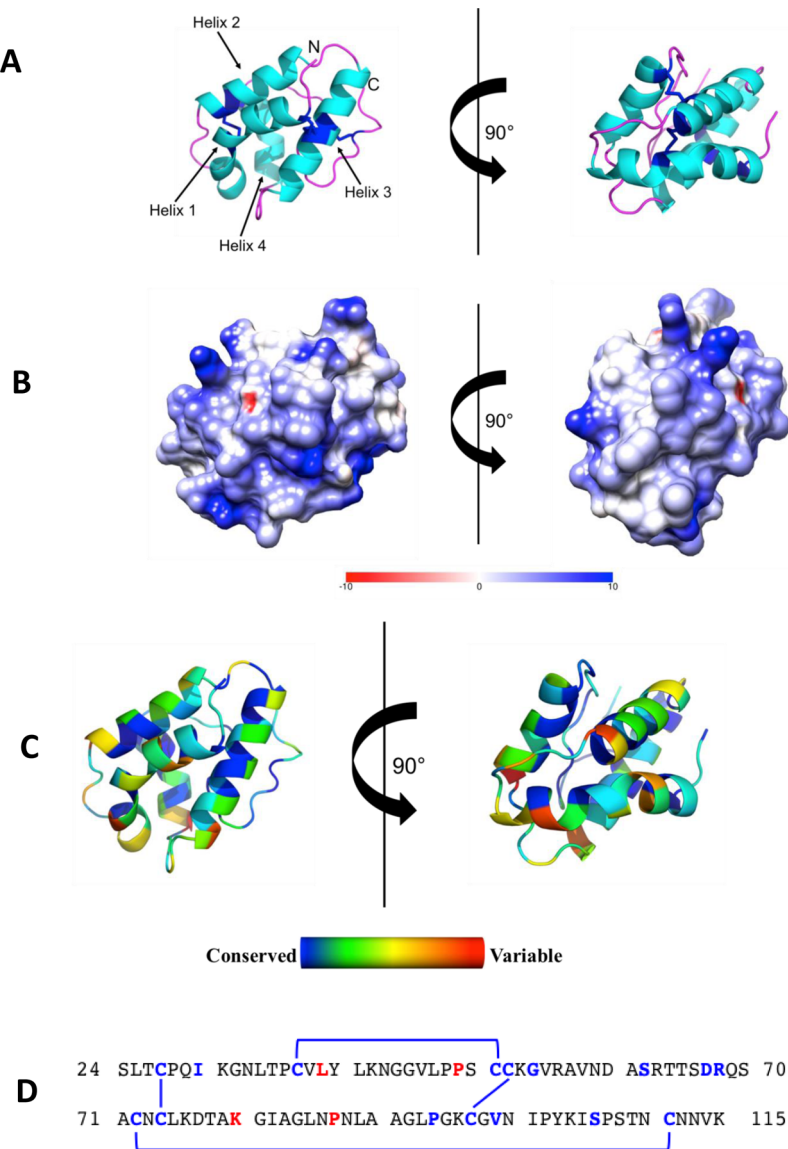


Figure 3. (A) Overall structure of Cor a 8. Secondary structural elements are colored separately where α -helices are cyan, β -sheets are red, loops are magenta, and disulfide bonds are blue. (B) Surface representation of Cor a 8 with electrostatic potentials where blue indicates positive charge and red indicates negative charge in units of kcal/(mol·e). (C) Ribbon representation of Cor a 8 showing conserved residues derived from an alignment of 150 Cor a 8-related protein sequences selected by ConSurf. The most conserved residues are shown in blue, whereas the most variable residues are shown in red. (D) Sequence of Cor a 8, in which the most conserved residues are blue and the most variable residues are red. The cysteine residues participating in disulfide linkages are bracketed.

PAGE analysis revealed that fractions F21–F24 were highly enriched in a protein with a molecular mass of \sim 14000 Da (Figure 1A). Upon reduction, a band of about 12000 Da became visible (Figure 1B). This higher apparent molecular weight in SDS-PAGE seems to be characteristic for nsLTPs, as it was also shown for other members of this protein family.^{22,49} MALDI-TOF-MS analysis yielded a mass of 9473.1 Da ($[M + H]^+ = 9475.8$; $[M + 2H]^{2+} = 4736.7$) (Figure 1C), which is in good correlation with the theoretical mass of 9468.0 Da (Uniprot Q9ATH2, aa 24–115). Further evidence came from the N-terminal sequencing, which confirmed the first six N-terminal amino acid residues (SLTCPQ).

Secondary Structure and Thermostability. The overall secondary structural composition and heat stability were investigated using CD spectroscopy (Figure 2). CD spectra of the native protein at room temperature showed the typical

characteristics of nsLTPs with high α -helical content. At room temperature, differences in pH did not change the secondary structure. However, the spectra of Cor a 8 prior to and after heating at pH 7.5 were different, showing that thermal unfolding was irreversible, whereas at pH 2.5 the overall protein fold was partially recovered. This demonstrates that Cor a 8 is more stable at acidic than at neutral conditions.

Structural Analysis of Cor a 8. The full-length, immature, Cor a 8 molecule is composed of 115 residues; residues 1–23 correspond to the signal peptide, which is cleaved upon maturation. All residues that comprise the mature protein, 24–115, are visible in the electron density map in both chains A and B. Overall, the mature Cor a 8 molecule is composed of four α -helices connected by loop regions. Eight cysteine residues are present in the mature protein, all of which participate in disulfide bonds: residues 27 and 74, 37 and 51, 52 and 97, and 72 and 111

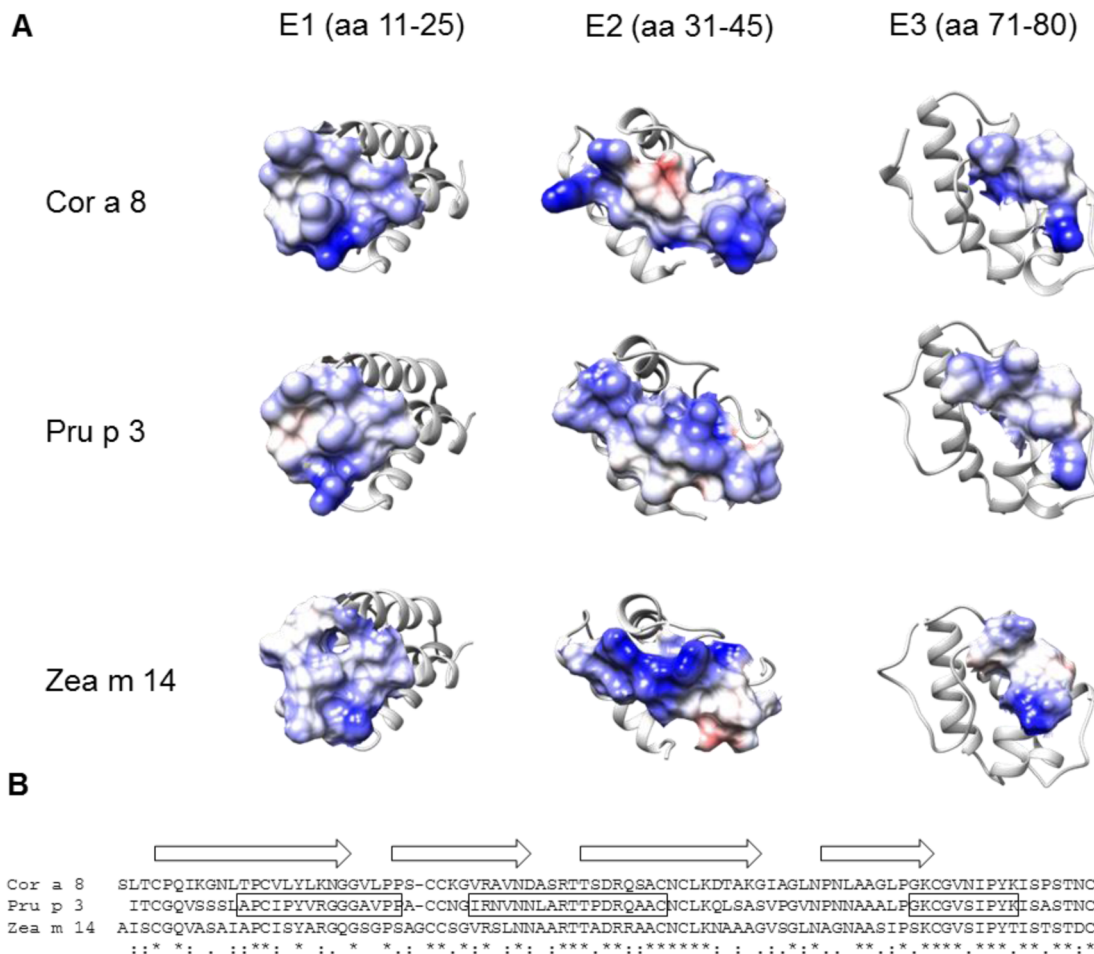


Figure 4. (A) Comparison of known epitope surface regions between Cor a 8, Pru p 3, and Zea m 14 (maize nsLTP); surface representation with electrostatic potentials where blue indicates positive charge and red indicates negative charge in units of kcal/(mol·e). (B) Primary sequence alignment of the mature protein sequences of Cor a 8, Pru p 3, and Zea m 14. Arrows indicate α -helices, and previously identified IgE-binding epitopes of Pru p 3 are marked with boxes.

(Figure 3). A comparison of chains A and B reveals very slight differences between the two, namely, at residues 64–68, 86–89, and 112–115. Chains A and B superpose with a root-mean-square deviation (RMSD) of 0.4 Å over 92 aligned Ca atoms. Although Cor a 8 crystallized with two subunits per asymmetric unit, PDBePISA suggests that this protein is monomeric. Electrostatic potentials were calculated using Chimera and are mapped out on the surface of Cor a 8, shown in Figure 3B.

Structural Comparison of Cor a 8 with Other Members of the nsLTP-family. Upon performing a search to find

structurally similar proteins to Cor a 8, the Dali server identified the nsLTP Pru p 3 from peach (PDB ID 2BSS) as the most closely related structure. A superposition of 2BSS on our structure results in a RMSD of 1.4 Å over 91 aligned C α atoms and a sequence identity of 57%. The peach allergen Pru p 3 (PDB ID 2BSS) has lauric acid bound in both subunits. A comparison of subunit A from Cor a 8 with subunit A of 2BSS reveals large structural differences at the C-terminus, residues 99–115 according to Cor a 8's numbering. Pru p 3's C-terminal loop is moved out toward the surface of the molecule, whereas the same region on Cor a 8 is closer to the core of the molecule. These changes are due to the binding of lauric acid between the third α -helix and the C-terminal loop of Pru p 3. Interestingly, a superposition of the two reveals that the pocket, where lauric acid is bound in the Pru p 3 structure, is occupied by Tyr103 of Cor a

8 (corresponding to Tyr79 of Pru p 3). The corresponding Tyr from Pru p 3 (Tyr79) is flipped outward, allowing for lauric acid to bind.

Dali also identified several nsLTPs from a variety of sources as structurally similar to Cor a 8. Aside from peach, an nsLTP from *Oryza sativa*, rice (for example, PDB ID 1UVC, RMSD value 1.2 Å over 90 aligned C α atoms, sequence identity of 48%), was identified as the second most structurally similar nsLTP to Cor a 8. 1UVC crystallized with two subunits per asymmetric unit. Each subunit has stearic acid bound, and it is bound to the core of the protein between all four α -helices. A comparison of subunit A from Cor a 8 with subunit A of 1UVC reveals no drastic structural changes between the two structures. There are slight conformational shifts in the α -helices, and the largest structural change is seen at the C-terminal loop, namely, residues 100–115 of Cor a 8 (which correspond to residues 76–91 of 1UVC).

Additionally, Dali identified nsLTPs from barley (for example, PDB ID 3GSH, RMSD value 1.2 Å over 90 aligned C α atoms, sequence identity of 43%) and maize nsLTP (*Zea m 14*; PDB ID 1MZL, RMSD value 1.4 Å over 92 aligned C α atoms, sequence identity of 48%) as structurally similar to Cor a 8. Barley nsLTP (3GSH) has an oxylipin adduct (PDB Ligand ID ASY) bound in both subunits. The adduct splits into two branches, where one branch is buried in the core of the protein between the first and third α -helix and the second branch interacts with the surface of

the protein at the third α -helix. This ligand's mode of binding is very different from that seen in both 2B5S and 1UVC. A superposition of Cor a 8 and 3GSH reveals slight structural differences with the largest conformational change located at the loop that connects helix 1 and helix 2. These differences, however, do not appear to be attributed to bound ligand. Zea m 14 (1MZL) is an apo nsLTP, like that of Cor a 8. A superposition of the two reveals differences in the loop region that connects helix 1 and helix 2, as well as differences in the loop that connects helix 3 and helix 4, and the differences continue on through the C-terminal loop. Furthermore, Dali identified nsLTPs from tobacco (PDB ID 1T12), mung bean (PDB ID 1SIY), and lentil (PDB ID 2MAL) as Cor a 8 related structures that have lower structural similarity than those listed above, but higher sequence identity, at >50% for all three. Figure 3C shows a ribbon representation of the Cor a 8 molecule, indicating conservation among 150 Cor a 8-related protein sequences selected by ConSurf. Furthermore, Figure 3D includes Cor a 8's sequence, where the most and least conserved residues are shown and disulfide linkages are indicated.

Figure 4 shows a comparison of the surface topology of relevant epitope regions of Pru p 3 (E1, aa 11–25; E2, aa 31–45; and E3, aa 71–80)²³ with that of Cor a 8 and Zea m 14. Despite a common backbone structure, differences in the surface topology, defined by the different side chains, are obvious. When E1 from Pru p 3 is compared to the respective areas of Cor a 8 and Zea m 14, the electrostatic potentials seem to be similar. In contrast, E2 from Pru p 3 lacks the negative charges present in Cor a 8 and Zea m 14. Epitope 3 seems to be predominantly neutral in Pru p 3 and Zea m 14, whereas Cor a 8 presents more positive charges in this area.

MD Simulations for Cor a 8. Overall, the structure of the MD relaxed model of the apo form of Cor a 8 is very similar to that seen in the crystal structure. RMSD calculated for all backbone atoms between the crystal structure and a representative snapshot amounts to 2.2 Å, with somewhat larger displacements for fragments 59–63 (2.6 Å), 77–87 (3.0 Å), and the C-terminal fragment 89–92 (3.2 Å). Conformations of the disulfide bridges are preserved throughout the simulated trajectory. For Tyr79, the same rotamer (CG–CB–CA–C ca. -80°) that is observed in the crystal structure prevails (88% of snapshots) during the 150 ns long trajectory. The side chain of Tyr79 remains mostly in hydrophobic regions of the interior of the protein with nearest neighbors Val35, Ser39, Ala48, Cys49, Leu52, and Ile78. Another rotamer of Tyr79 observed in the MD trajectory (12%; CG–CB–CA–C ca. 45°) also features the side chain buried in the hydrophobic interior of the protein.

To model the structure of a Cor a 8 with laureate bound, coordinates of laureate from the stable structure of the Pru p 3/laureate complex (vide infra) were merged with those for the protein from the crystal structure 4XUW. Throughout the whole trajectory laureate remained in this binding site, that is, in the middle of the protein between the four helices, whereas Tyr79 changed its conformation at the eighth ns of the simulation. More specifically, the dihedral angle CG–CB–CA–C changed its value from ca. -63° to ca. +45° (this is a minor (12%) rotamer of Tyr79 observed for the apo form of Cor a 8), which results in placing the phenolic ring of Tyr79 in contact with the aliphatic tail of laureate. Once this configuration was attained, it remained stable until the end of the simulated trajectory. RMSD calculated for all backbone atoms amounts to 1.7 Å, and a larger displacement with respect to the crystal structure was observed for the 76–87 fragment (3.2 Å). As in other simulations,

conformation of the disulfide bonds remains the same as in the crystal structure.

MD Simulations for Pru p 3/Pru p 3/Laureate/n-Heptane Complex. Simulation for Pru p 3 with laureate and *n*-heptane bound revealed the structure of the complex remains almost unchanged throughout the initial fragment (0–40 ns) of the simulated trajectory. Both ligands occupy the same sites as in the crystal structure, and Tyr79 is exposed at the protein surface. RMSD for the protein backbone calculated with respect to the crystal structure amounts to only 1.2 Å.

A clearly visible conformational change takes place between the 40th and 50th ns of the simulated trajectory, and it consists of movement of the 60–69 fragment (loop and helix) toward the 40–58 helix and simultaneous displacement of the *n*-heptane ligand from its original binding site toward the site originally occupied by laureate. Concertedly, Tyr79 moves into the protein's interior via changing its CG–CB–CA–C dihedral angle from around 180° to around -80°. RMSD for the backbone atoms is 1.85 Å with respect to the crystal structure, and larger differences are observed for fragment 60–69 (3.5 Å), which has moved during the conformational transition, and the C-terminal region 74–91 (2.4 Å). Laureate forms a salt bridge with Arg32, whereas its aliphatic tail takes the place occupied by *n*-heptane in the crystal structure.

Pru p 3/Laureate Complex. The initial geometry of the Pru p 3/laureate complex was obtained by removal of *n*-heptane from the crystal structure (2B5S). After simulations, the overall structure of the protein is very similar to that observed in the crystal; RMSD for all backbone atoms amounts to 1.3 Å, and it is slightly larger for the loop 19–23 (1.7 Å) and fragments 75–86 (2.0 Å) and 86–92 (2.0 Å). Notably, at a fairly early stage of the MD simulation (around 37 ns), the laureate moved from its initial binding site to the site in the middle of the protein, that is, between the four helices, which was previously occupied by *n*-heptane, and it remained in this pocket until the end of the trajectory (150 ns). Once the laureate moved deeper into the protein's interior, Tyr79 followed, finally attaining the same rotamer state as observed for a corresponding residue of Cor a 8.

Apo Pru p 3. Simulations for the apo form of Pru p 3 revealed the side chain of Tyr79 enters the hydrophobic interior of the protein within the first 2 ns of the simulation and later on this residue remains in the same rotamer state as observed for the Pru p 3/laureate complex. RMSD calculated for all backbone atoms with respect to the crystal structure is 2.7 Å; larger displacements are observed for fragments 60–69 (4.3 Å) and 74–91 (4.5 Å).

DISCUSSION

Nonspecific lipid transfer proteins are ubiquitously expressed throughout the plant kingdom, and a number of those have been identified to be important food allergens, such as Pru p 3 from peach, Mal d 3 from apple, and Act d 10 from kiwifruit. Immunological cross-reactivity is primarily due to shared 3D structures, accessible for IgE antibody recognition. However, despite their common structure, nsLTPs display low sequence identities and thus surface-exposed areas. Consequently, it was shown that members from distantly related species do not cross-react to the same extent as members within the same plant family.^{50,51} Therefore, structural analysis of individual nsLTPs provides detailed information for allergenic risk assessment.

Purified natural Cor a 8 crystallized in a monoclinic crystal form with an extremely low solvent content of 28% and a Matthews coefficient of 1.71 Å³ Da⁻¹. These circumstances may contribute to how well the crystal diffracted, because crystals with

lower solvent content tend to diffract better.⁵² Notably, the structure of Cor a 8 reported here (PDB ID 4XUW) is one of the most tightly packed structures reported to the PDB.⁵³ Cor a 8 is the first hazelnut allergen with its structure determined, and the high-resolution model that was obtained provides a very accurate template for in silico analysis of IgE cross-reactivity among Cor a 8 and other nsLTPs.

Moreover, it was shown that the allergen is more stable in an acidic environment, enabling proper refolding post thermal denaturation. These results are in good correlation with a study from Gaier et al., who showed that natural Pru p 3 is more stable under acidic conditions as compared to neutral ones.⁵⁴ The authors discuss that cleavage of disulfide bonds at neutral pH and high temperature is due to β -elimination, a reaction in which a base-catalyzed subtraction of a β -proton from a cysteine results in cleavage of disulfide bonds, which was shown for thaumatin.

Molecular dynamics simulations performed for apo- and laureate-bound forms of Cor a 8 and Pru p 3 and the laureate/*n*-heptane double complex of Pru p 3 revealed several structural features of these proteins. First, the preferred site for binding a hydrophobic ligand is located in the center of the protein's core. Second, only when two ligands are bound simultaneously, as in the 2BSS crystal structure of Pru p 3, can the Tyr79 side chain be exposed at the surface of the protein as it can be expelled from the hydrophobic interior by the second ligand. Extended MD simulation for Pru p 3/laureate/*n*-heptane complex indicates, however, that binding of two ligands is not enough to force Tyr79 out, as with binding the two ligands differently (laureate and *n*-heptane swapped and laureate bound more shallowly) Tyr79 attains a rotameric state with its side chain pointing toward the protein's core. In apo forms of the proteins and in complexes with one (laureate) ligand, the Tyr79 side chain is buried in the interior of the protein, where it lines up a substrate pocket.

Two distinctive conformational states have been observed for Pru p 3, an open conformation, which is stable when a hydrophobic ligand occupies a bottom of the substrate pocket in the center of the protein (lined up by Leu10, Cys13-Cys27, Ile14, Val17, Ala66, and Leu69 side chains). This conformation is observed in the crystal structure 2BSS, as well as in the MD simulation for the Pru p 3/laureate complex. When a ligand binds more shallowly, or it is missing completely, the 62–74 helix moves toward the 40–58 helix and a closed conformation forms. No such easily noticeable conformational changes take place upon laureate binding to Cor a 8.

Although the overall structure of nsLTPs is highly conserved, sequence identities among nsLTPs are rather low, showing different degrees of identity among different sources. Members from the Rosaceae family (peach, apple, and almond), for example, show closely related primary structures (88–97% identity), whereas nsLTPs from more distantly related plant species such as seeds, cereals, or pollens are clearly less similar to the Rosaceae allergens, as well as to each other. Borges et al. showed that, on the basis of their relatively high sequence identities, nsLTPs from Rosaceae share consensus epitopes responsible for their IgE-binding cross-reactivity.⁵⁵ However, despite their high structural conservation, it seems that nsLTPs from distantly related species do not cross-react to the same extent as members belonging to the Rosaceae family.^{22,24} Cross-inhibition experiments indicate that Pru p 3 was able to at least diminish binding to other members of the nsLTP family.²⁴

To get a better understanding of the structural determinants relevant for IgE cross-reactivity, we compared the obtained three-dimensional structure of Cor a 8 with known structures of other

nsLTPs. Figure 4 shows a comparison of already defined Pru p 3 epitope regions²³ with the corresponding regions from Cor a 8 and Zea m 14. Differences observed in the surface topology, defined by the different side chains, became obvious (Figure 4). Focusing on the electrostatic potentials, these areas demonstrated that differences between Cor a 8 and Pru p 3 were lower as compared to differences between Pru p 3 and maize LTP. Thus, it seems that the occurrence of IgE cross-reactive epitopes is based on the degree of surface topology, dependent on side chains, which are determinants of the allergen–antibody interaction. Since the exposed residues are based on the primary sequence, one could conclude that the degree of IgE cross-reactivity between different members of the nsLTP family depends on similarities of the respective epitope region, defining the molecular surface. This finding correlates with data from a recent study by Morales et al.,²⁴ who demonstrated that Pru p 3 shares some common epitopes with other nsLTPs, such as Cor a 8, Mal d 3, and Zea m 14. However, no complete inhibition was observed in cross-reactivity studies. This is in accordance with data from Hartz et al., who identified patients with allergic reactions to hazelnut but tolerant for peach.²³

Currently, only a small fraction of food allergens have their structures determined experimentally. However, it is evident that only "real" structures help us to identify relevant surface-exposed areas, which are important for antibody binding and recognition. Furthermore, obtaining structural data from distantly related members of a protein family allow for more refined/reliable predictions for the range of cross-reactivities, with and without clinical implications. In addition, this information will contribute to the development of molecules with a reduced allergenic activity that would allow for a safer immunotherapeutic approach. As a first step we think that this newly identified Cor a 8 structure will help to elucidate the range of cross-reactivity and major IgE epitopes within the nsLTP family.

ASSOCIATED CONTENT

Accession Codes

Coordinates and structure factors have been deposited to the PDB with the following accession code: 4XUW.

AUTHOR INFORMATION

Corresponding Authors

*(M.C.) Phone: (803) 777-7399. Fax: (803) 777-9521. E-mail: chruszcz@mailbox.sc.edu.

*(K.H.-S.) Phone: +43 1 40400 51040. Fax: +43 1 40400 51300. E-mail: karin.hoffmann@meduniwien.ac.at.

Funding

This work is partially supported by an ASPIRE grant from the Office of the Vice President of Research at the University of South Carolina. Further support came from the Austrian Science Fund (FWF: SFB F4603 and W1248). This research was additionally supported in part by PL-Grid Infrastructure.

Notes

The authors declare no competing financial interest.

ACKNOWLEDGMENTS

Data were collected at Southeast Regional Collaborative Access Team (SER-CAT) 22-BM beamline at the Advanced Photon Source, Argonne National Laboratory. Supporting institutions may be found at www.ser-cat.org/members.html. Use of the Advanced Photon Source was supported by the U.S. Department

of Energy, Office of Science, Office of Basic Energy Sciences, under Contract W-31-109-Eng-38.

ABBREVIATIONS USED

ANL, Argonne National Laboratory; APS, Advanced Photon Source; AU, asymmetric unit cell; CD, circular dichroism; MALDI-TOF-MS, matrix-assisted laser desorption ionization–time of flight–mass spectrometry; nsLTP, nonspecific lipid transfer protein; PDB, Protein Data Bank; RMSD, root-mean-square deviation; SDS, sodium dodecyl sulfate

REFERENCES

- (1) Muraro, A.; Werfel, T.; Hoffmann-Sommergruber, K.; Roberts, G.; Beyer, K.; Bindsev-Jensen, C.; Cardona, V.; Dubois, A.; duToit, G.; Eigenmann, P.; Fernandez Rivas, M.; Halken, S.; Hickstein, L.; Host, A.; Knol, E.; Lack, G.; Marchisotto, M. J.; Niggemann, B.; Nwari, B. I.; Papadopoulos, N. G.; Poulsen, L. K.; Santos, A. F.; Skypala, I.; Schoepfer, A.; Van Ree, R.; Venter, C.; Worm, M.; Vlieg-Boerstra, B.; Panesar, S.; de Silva, D.; Soares-Weiser, K.; Sheikh, A.; Ballmer-Weber, B. K.; Nilsson, C.; de Jong, N. W.; Akdis, C. A. EAACI food allergy and anaphylaxis guidelines: diagnosis and management of food allergy. *Allergy* **2014**, *69*, 1008–1025.
- (2) Nwari, B. I.; Hickstein, L.; Panesar, S. S.; Roberts, G.; Muraro, A.; Sheikh, A. Prevalence of common food allergies in Europe: a systematic review and meta-analysis. *Allergy* **2014**, *69*, 992–1007.
- (3) De Knop, K. J.; Verweij, M. M.; Grimmelikhuijsen, M.; Philips, E.; Hagendorens, M. M.; Bridts, C. H.; De Clerck, L. S.; Stevens, W. J.; Ebo, D. G. Age-related sensitization profiles for hazelnut (*Corylus avellana*) in a birch-endemic region. *Ped. Allergy Immunol.* **2011**, *22*, e139–149.
- (4) Hansen, K. S.; Ballmer-Weber, B. K.; Sastre, J.; Lidholm, J.; Andersson, K.; Oberhofer, H.; Lluch-Bernal, M.; Ostling, J.; Mattsson, L.; Schocker, F.; Vieths, S.; Poulsen, L. K. Component-resolved in vitro diagnosis of hazelnut allergy in Europe. *J. Allergy Clin. Immunol.* **2009**, *123*, 1134–1141.
- (5) Sicherer, S. H.; Munoz-Furlong, A.; Godbold, J. H.; Sampson, H. A. US prevalence of self-reported peanut, tree nut, and sesame allergy: 11-year follow-up. *J. Allergy Clin. Immunol.* **2010**, *125*, 1322–1326.
- (6) Burney, P. G.; Potts, J.; Kummeling, I.; Mills, E. N.; Clausen, M.; Dubakiene, R.; Barreales, L.; Fernandez-Perez, C.; Fernandez-Rivas, M.; Le, T. M.; Knulst, A. C.; Kowalski, M. L.; Lidholm, J.; Ballmer-Weber, B. K.; Braun-Fahlander, C.; Mustakov, T.; Kralimarkova, T.; Popov, T.; Sakellarou, A.; Papadopoulos, N. G.; Versteeg, S. A.; Zuidmeer, L.; Akkerdaas, J. H.; Hoffmann-Sommergruber, K.; van Ree, R. The prevalence and distribution of food sensitization in European adults. *Allergy* **2014**, *69*, 365–371.
- (7) Radauer, C.; Nandy, A.; Ferreira, F.; Goodman, R. E.; Larsen, J. N.; Lidholm, J.; Pomes, A.; Rauf-Haimsoth, M.; Rozynek, P.; Thomas, W. R.; Breiteneder, H. Update of the WHO/IUIS Allergen Nomenclature Database based on analysis of allergen sequences. *Allergy* **2014**, *69*, 413–419.
- (8) Luttkopf, D.; Muller, U.; Skov, P. S.; Ballmer-Weber, B. K.; Wuthrich, B.; Skamstrup Hansen, K.; Poulsen, L. K.; Kastner, M.; Haustein, D.; Vieths, S. Comparison of four variants of a major allergen in hazelnut (*Corylus avellana*) Cor a 1.04 with the major hazel pollen allergen Cor a 1.01. *Mol. Immunol.* **2002**, *38*, 515–525.
- (9) Pastorello, E. A.; Vieths, S.; Pravettoni, V.; Farioli, L.; Trambaioli, C.; Fortunato, D.; Luttkopf, D.; Calamari, M.; Ansaldi, R.; Scibilia, J.; Ballmer-Weber, B. K.; Poulsen, L. K.; Wutrich, B.; Hansen, K. S.; Robino, A. M.; Ortolani, C.; Conti, A. Identification of hazelnut major allergens in sensitive patients with positive double-blind, placebo-controlled food challenge results. *J. Allergy Clin. Immunol.* **2002**, *109*, 563–570.
- (10) Faber, M. A.; De Graag, M.; Van Der Heijden, C.; Sabato, V.; Hagendorens, M. M.; Bridts, C. H.; De Clerck, L. S.; Ebo, D. G. Cor a 14: missing link in the molecular diagnosis of hazelnut allergy? *Int. Arch. Allergy Immunol.* **2014**, *164*, 200–206.
- (11) Verweij, M. M.; Hagendorens, M. M.; Trashin, S.; Cucu, T.; De Meulenaeer, B.; Devreese, B.; Bridts, C. H.; De Clerck, L. S.; Ebo, D. G. Age-dependent sensitization to the 7S-vicilin-like protein Cor a 11 from hazelnut (*Corylus avellana*) in a birch-endemic region. *J. Invest. Allerg. Clin. Immunol.* **2012**, *22*, 245–251.
- (12) Masthoff, L. J.; Mattsson, L.; Zuidmeer-Jongejan, L.; Lidholm, J.; Andersson, K.; Akkerdaas, J. H.; Versteeg, S. A.; Garino, C.; Meijer, Y.; Kentie, P.; Versluis, A.; den Hartog Jager, C. F.; Bruijnzeel-Koomen, C. A.; Knulst, A. C.; van Ree, R.; van Hoffen, E.; Pasman, S. G. Sensitization to Cor a 9 and Cor a 14 is highly specific for a hazelnut allergy with objective symptoms in Dutch children and adults. *J. Allergy Clin. Immunol.* **2013**, *132*, 393–399.
- (13) Schocker, F.; Luttkopf, D.; Scheurer, S.; Petersen, A.; Cistero-Bahima, A.; Enrique, E.; San Miguel-Moncin, M.; Akkerdaas, J.; van Ree, R.; Vieths, S.; Becker, W. M. Recombinant lipid transfer protein Cor a 8 from hazelnut: a new tool for in vitro diagnosis of potentially severe hazelnut allergy. *J. Allergy Clin. Immunol.* **2004**, *113*, 141–147.
- (14) Flinterman, A. E.; Akkerdaas, J. H.; den Hartog Jager, C. F.; Rigby, N. M.; Fernandez-Rivas, M.; Hoekstra, M. O.; Bruijnzeel-Koomen, C. A.; Knulst, A. C.; van Ree, R.; Pasman, S. G. Lipid transfer protein-linked hazelnut allergy in children from a non-Mediterranean birch-endemic area. *J. Allergy Clin. Immunol.* **2008**, *121*, 423–428.
- (15) Yeats, T. H.; Rose, J. K. The biochemistry and biology of extracellular plant lipid-transfer proteins (LTPs). *Protein Sci.* **2008**, *17*, 191–198.
- (16) Salcedo, G.; Sanchez-Monge, R.; Barber, D.; Diaz-Perales, A. Plant non-specific lipid transfer proteins: an interface between plant defence and human allergy. *Biochim. Biophys. Acta, Mol. Cell Biol. Lipids* **2007**, *1771*, 781–791.
- (17) Douliez, J. P.; Michon, T.; Elmorjani, K.; Marion, D. Structure, biological and technological functions of lipid transfer proteins and indolines, the major lipid binding proteins from cereal kernels. *J. Cereal Sci.* **2000**, *32*, 1–20.
- (18) Kader, J. C.; Julienne, M.; Vergnolle, C. Purification and characterization of a spinach-leaf protein capable of transferring phospholipids from liposomes to mitochondria or chloroplasts. *Eur. J. Biochem.* **1984**, *139*, 411–416.
- (19) Sy, D.; Le Gravier, Y.; Goodfellow, J.; Vovelle, F. Protein stability and plasticity of the hydrophobic cavity in wheat ns-LTP. *J. Biomol. Struct. Dyn.* **2003**, *21*, 15–29.
- (20) Asero, R.; Mistrello, G.; Roncarolo, D.; de Vries, S. C.; Gautier, M. F.; Ciurana, C. L.; Verbeek, E.; Mohammadi, T.; Knul-Brettova, V.; Akkerdaas, J. H.; Bulder, I.; Aalberse, R. C.; van Ree, R. Lipid transfer protein: a pan-allergen in plant-derived foods that is highly resistant to pepsin digestion. *Int. Arch. Allergy Immunol.* **2000**, *122*, 20–32.
- (21) Lindorff-Larsen, K.; Winther, J. R. Surprisingly high stability of barley lipid transfer protein, LTP1, towards denaturant, heat and proteases. *FEBS Lett.* **2001**, *488*, 145–148.
- (22) Diaz-Perales, A.; Lombardero, M.; Sanchez-Monge, R.; Garcia-Selles, F. J.; Pernas, M.; Fernandez-Rivas, M.; Barber, D.; Salcedo, G. Lipid-transfer proteins as potential plant panallergens: cross-reactivity among proteins of *Artemisia* pollen, *Castanea* nut and Rosaceae fruits, with different IgE-binding capacities. *Clin. Exp. Allergy* **2000**, *30*, 1403–1410.
- (23) Hartz, C.; Lauer, I.; del Mar San Miguel Moncin, M.; Cistero-Bahima, A.; Foetisch, K.; Lidholm, J.; Vieths, S.; Scheurer, S. Comparison of IgE-binding capacity, cross-reactivity and biological potency of allergenic non-specific lipid transfer proteins from peach, cherry and hazelnut. *Int. Arch. Allergy Immunol.* **2010**, *153*, 335–346.
- (24) Morales, M.; Lopez-Matas, M. A.; Moya, R.; Carnes, J. Cross-reactivity among non-specific lipid-transfer proteins from food and pollen allergenic sources. *Food Chem.* **2014**, *165*, 397–402.
- (25) Otwinowski, Z.; Minor, W. Processing of X-ray diffraction data collected in oscillation mode. *Methods Enzymol.* **1997**, *276*, 307–326.
- (26) Minor, W.; Cymborowski, M.; Otwinowski, Z.; Chruszcz, M. HKL-3000: the integration of data reduction and structure solution – from diffraction images to an initial model in minutes. *Acta Crystallogr., Sect. D: Biol. Crystallogr.* **2006**, *62*, 859–866.
- (27) Vagin, A.; Teplyakov, A. MOLREP: an automated program for molecular replacement. *J. Appl. Crystallogr.* **1997**, *30*, 1022–1025.

- (28) Winn, M. D.; Ballard, C. C.; Cowtan, K. D.; Dodson, E. J.; Emsley, P.; Evans, P. R.; Keegan, R. M.; Krissinel, E. B.; Leslie, A. G.; McCoy, A.; McNicholas, S. J.; Murshudov, G. N.; Pannu, N. S.; Potterton, E. A.; Powell, H. R.; Read, R. J.; Vagin, A.; Wilson, K. S. Overview of the CCP4 suite and current developments. *Acta Crystallogr., Sect. D: Biol. Crystallogr.* **2011**, *67*, 235–242.
- (29) Emsley, P.; Cowtan, K. Coot: model-building tools for molecular graphics. *Acta Crystallogr., Sect. D: Biol. Crystallogr.* **2004**, *60*, 2126–2132.
- (30) Cowtan, K. The Buccaneer software for automated model building. 1. Tracing protein chains. *Acta Crystallogr., Sect. D: Biol. Crystallogr.* **2006**, *62*, 1002–1011.
- (31) Perrakis, A.; Morris, R.; Lamzin, V. S. Automated protein model building combined with iterative structure refinement. *Nat. Struct. Biol.* **1999**, *6*, 458–463.
- (32) Murshudov, G. N.; Skubak, P.; Lebedev, A. A.; Pannu, N. S.; Steiner, R. A.; Nicholls, R. A.; Winn, M. D.; Long, F.; Vagin, A. A. REFMAC5 for the refinement of macromolecular crystal structures. *Acta Crystallogr., Sect. D: Biol. Crystallogr.* **2011**, *67*, 355–367.
- (33) Davis, I. W.; Leaver-Fay, A.; Chen, V. B.; Block, J. N.; Kapral, G. J.; Wang, X.; Murray, L. W.; Arendall, W. B., 3rd; Snoeyink, J.; Richardson, J. S.; Richardson, D. C. MolProbity: all-atom contacts and structure validation for proteins and nucleic acids. *Nucleic Acids Res.* **2007**, *35*, W375–383.
- (34) Yang, H.; Guranovic, V.; Dutta, S.; Feng, Z.; Berman, H. M.; Westbrook, J. D. Automated and accurate deposition of structures solved by X-ray diffraction to the Protein Data Bank. *Acta Crystallogr., Sect. D: Biol. Crystallogr.* **2004**, *60*, 1833–1839.
- (35) Frisch, M. J.; Trucks, G. W.; Schlegel, H. B.; Scuseria, G. E.; Robb, M. A.; Cheeseman, J. R.; Scalmani, G.; Barone, V.; Mennucci, B.; Petersson, G. A.; Nakatsuji, H.; Caricato, M.; Li, X.; Hratchian, H. P.; Izmaylov, A. F.; Bloino, J.; Zheng, G.; Sonnenberg, J. L.; Hada, M.; Ehara, M.; Toyota, K.; Fukuda, R.; Hasegawa, J.; Ishida, M.; Nakajima, T.; Honda, Y.; Kitao, O.; Nakai, H.; Vreven, T.; Montgomery, J. A., Jr.; Peralta, J. E.; Ogliaro, F.; Bearpark, M. J.; Heyd, J.; Brothers, E. N.; Kudin, K. N.; Staroverov, V. N.; Kobayashi, R.; Normand, J.; Raghavachari, K.; Rendell, A. P.; Burant, J. C.; Iyengar, S. S.; Tomasi, J.; Cossi, M.; Rega, N.; Millam, N. J.; Klene, M.; Knox, J. E.; Cross, J. B.; Bakken, V.; Adamo, C.; Jaramillo, J.; Gomperts, R.; Stratmann, R. E.; Yazyev, O.; Austin, A. J.; Cammi, R.; Pomelli, C.; Ochterski, J. W.; Martin, R. L.; Morokuma, K.; Zakrzewski, V. G.; Voth, G. A.; Salvador, P.; Dannenberg, J. J.; Dapprich, S.; Daniels, A. D.; Farkas, Ö.; Foresman, J. B.; Ortiz, J. V.; Cioslowski, J.; Fox, D. J. Gaussian 09; Gaussian, Inc.: Wallingford, CT, USA, 2009.
- (36) Case, D. A.; Cheatham, T. E., 3rd; Darden, T.; Gohlke, H.; Luo, R.; Merz, K. M., Jr.; Onufriev, A.; Simmerling, C.; Wang, B.; Woods, R. J. The Amber biomolecular simulation programs. *J. Comput. Chem.* **2005**, *26*, 1668–1688.
- (37) Olsson, M. H. M.; Sondergaard, C. R.; Rostkowski, M.; Jensen, J. H. PROPKA3: consistent treatment of internal and surface residues in empirical pK(a) predictions. *J. Chem. Theory Comput.* **2011**, *7*, 525–537.
- (38) Jorgensen, W. L.; Chandrasekhar, J.; Madura, J. D.; Impey, R. W.; Klein, M. L. Comparison of simple potential functions for simulating liquid water. *J. Chem. Phys.* **1983**, *79*, 926–935.
- (39) Case, D. A.; Darden, T. A.; Cheatham, T. E.; Simmerling, C. L.; Wang, J.; Duke, R. E.; Luo, R.; Walker, R. C.; Zhang, W.; Merz, K. M.; Roberts, B.; Hayik, S.; Roitberg, A.; Seabra, G.; Swails, J.; Goetz, A. W.; Kolossváry, I.; Wong, K. F.; Paesani, F.; Vanicek, J.; Wolf, R. M.; Liu, J.; Wu, X.; Brozell, S. R.; Steinbrecher, T.; Gohlke, H.; Cai, Q.; Ye, X.; Wang, J.; Hsieh, M. J.; Cui, G.; Roe, D. R.; Mathews, D. H.; Seetin, M. G.; Salomon-Ferrer, R.; Sagui, C.; Babin, V.; Luchko, T.; Gusarov, S.; Kovalenko, A.; Kollman, P. A. AMBER 12; University of California, San Francisco, CA, USA, 2012.
- (40) Salomon-Ferrer, R.; Gotz, A. W.; Poole, D.; Le Grand, S.; Walker, R. C. Routine microsecond molecular dynamics simulations with AMBER on GPUs. 2. Explicit solvent particle mesh Ewald. *J. Chem. Theory Comput.* **2013**, *9*, 3878–3888.
- (41) Painter, J.; Merritt, E. A. mmLib Python toolkit for manipulating annotated structural models of biological macromolecules. *J. Appl. Crystallogr.* **2004**, *37*, 174–178.
- (42) Painter, J.; Merritt, E. A. A molecular viewer for the analysis of TLS rigid-body motion in macromolecules. *Acta Crystallogr., Sect. D: Biol. Crystallogr.* **2005**, *61*, 465–471.
- (43) Krissinel, E.; Henrick, K. Secondary-structure matching (SSM), a new tool for fast protein structure alignment in three dimensions. *Acta Crystallogr., Sect. D: Biol. Crystallogr.* **2004**, *60*, 2256–2268.
- (44) DeLano, W. L. PyMOL Molecular Graphics System, 2010
- (45) Pettersen, E. F.; Goddard, T. D.; Huang, C. C.; Couch, G. S.; Greenblatt, D. M.; Meng, E. C.; Ferrin, T. E. UCSF Chimera—a visualization system for exploratory research and analysis. *J. Comput. Chem.* **2004**, *25*, 1605–1612.
- (46) Krissinel, E.; Henrick, K. Inference of macromolecular assemblies from crystalline state. *J. Mol. Biol.* **2007**, *372*, 774–797.
- (47) Holm, L.; Rosenstrom, P. DALI server: conservation mapping in 3D. *Nucleic Acids Res.* **2010**, *38*, W545–549.
- (48) Ashkenazy, H.; Erez, E.; Martz, E.; Pupko, T.; Ben-Tal, N. ConSurf 2010: calculating evolutionary conservation in sequence and structure of proteins and nucleic acids. *Nucleic Acids Res.* **2010**, *38*, W529–533.
- (49) Sanchez-Monge, R.; Lombardero, M.; Garcia-Selles, F. J.; Barber, D.; Salcedo, G. Lipid-transfer proteins are relevant allergens in fruit allergy. *J. Allergy Clin. Immunol.* **1999**, *103*, 514–519.
- (50) Hartz, C.; Lauer, I.; del Mar San Miguel Moncin, M.; Cistero-Bahima, A.; Foetisch, K.; Lidholm, J.; Vieths, S.; Scheurer, S. Comparison of IgE-binding capacity, cross-reactivity and biological potency of allergenic non-specific lipid transfer proteins from peach, cherry and hazelnut. *Int. Arch. Allergy Immunol.* **2010**, *153*, 335–346.
- (51) Morales, M.; Lopez-Matas, M. A.; Moya, R.; Carnes, J. Cross-reactivity among non-specific lipid-transfer proteins from food and pollen allergenic sources. *Food Chem.* **2014**, *165*, 397–402.
- (52) Kantardjieff, K. A.; Rupp, B. Matthews coefficient probabilities: Improved estimates for unit cell contents of proteins, DNA, and protein-nucleic acid complex crystals. *Protein Sci.* **2003**, *12*, 1865–1871.
- (53) Trillo-Muyo, S.; Jasilonis, A.; Domagalski, M. J.; Chruszcz, M.; Minor, W.; Kuisiene, N.; Arolas, J. L.; Sola, M.; Gomis-Ruth, F. X. Ultratight crystal packing of a 10 kDa protein. *Acta Crystallogr., Sect. D: Biol. Crystallogr.* **2013**, *69*, 464–470.
- (54) Gaier, S.; Marsh, J.; Oberhuber, C.; Rigby, N. M.; Lovegrove, A.; Alessandri, S.; Briza, P.; Radauer, C.; Zuidmeer, L.; van Ree, R.; Hemmer, W.; Sancho, A. I.; Mills, C.; Hoffmann-Sommergruber, K.; Shewry, P. R. Purification and structural stability of the peach allergens Pru p 1 and Pru p 3. *Mol. Nutr. Food Res.* **2008**, *52* (Suppl. 2), S220–S229.
- (55) Borges, J. P.; Barre, A.; Culquerier, R.; Granier, C.; Didier, A.; Rouge, P. Lipid transfer proteins from Rosaceae fruits share consensus epitopes responsible for their IgE-binding cross-reactivity. *Biochem. Biophys. Res. Commun.* **2008**, *365*, 685–690.